Available online at www.sciencedirect.com
ScienceDirect
Journal of Solid State Chemistry 180 (2007) 1110–1118
JOURNAL OF SOLID STATE CHEMISTRY
www.elsevier.com/locate/jssc

$AgGaS_2$-type photocatalysts for hydrogen production under visible light: Effects of post-synthetic H_2S treatment

Jum Suk Jang[a], Sun Hee Choi[b], Namsoo Shin[b], Chungjong Yu[b], Jae Sung Lee[a,*]

[a]*Eco-friendly Catalysis and Energy Laboratory (NRL), Department of Chemical Engineering, School of Environmental Science and Engineering*
[b]*Beamline Research Division, Pohang Accelerator Laboratory, Pohang University of Science and Technology (POSTECH), San 31, Hyojadong, Namgu, Pohang 790-784, Republic of Korea*

Received 10 November 2006; received in revised form 29 December 2006; accepted 5 January 2007
Available online 21 January 2007

Abstract

Bulky $AgGaS_2$ was synthesized as a p-type semiconductor photocatalyst by a conventional solid state reaction under N_2 flow for hydrogen production under visible light. To remove impurity phases involved in the synthesized material and improve crystallinity, the material was treated at various temperatures of 873–1123 K under H_2S flow. Impurity phases were identified as β-Ga_2O_3 and Ag_9GaS_6 with the cell refinements of XRD and the local coordination structure around gallium atom in $AgGaS_2$ was investigated by EXAFS. As the H_2S-treatment temperature increased, the contribution from impurity phases was diminished. When the temperature reached 1123 K, the impurity phases were completely removed and the material showed the highest photocatalytic activity. Thus, the post-synthetic H_2S treatment could be applied for the synthesis of sulfide-type photocatalysts with high activity.

Keywords: $AgGaS_2$; Photocatalyst; Visible light; Hydrogen production; H_2S treatment

1. Introduction

Sulfide photocatalysts have been known to be active for hydrogen production from aqueous electrolyte solutions containing a sacrificial electron donor (Na_2S or/and Na_2SO_3) under visible light irradiation [1,2]. In an environmental application, these photocatalysts could be used for decomposition of the harmful H_2S gas absorbed in alkaline water without such sacrificial electron donors [3,4]. In contrast to oxide photocatalysts [5,6], the band gap energy and band positions of sulfide photocatalysts can drive both oxidation and reduction of water under visible light irradiation. The single component metal sulfide such as CdS is usually not very active in hydrogen production, and subject to photo-corrosion [7]. On the contrary, the multicomponent metal sulfides such as chalcogenide (AB_2X_4) and chalcopyrite (ABX_2) are more stable and show higher photocatalytic activity under visible light [8–10]. $AgGaS_2$ is a p-type material of I–III–VI ternary semiconductors, which crystallize in the chalcopyrite structure. It has a direct band gap of ca. 2.68 eV and has become a promising material for solar cells, non-linear optical devices and blue light-emitting diodes (LED) [10–13]. But, it has also been reported that vacancies or interstitial defects in the chalcopyrite lattice cause these materials to have poor crystal quality and optical property [14].

In this work, bulky $AgGaS_2$ was prepared by a conventional solid-state reaction at various temperatures under N_2 flow. To remove the impurity phase and the defect which might cause a low photocatalytic activity for hydrogen production, the material was treated at elevated temperatures under H_2S flow. Before and after H_2S treatment, we investigated the structure of the materials mainly by synchrotron radiation techniques of X-ray diffraction and X-ray absorption fine structure (XAFS). The relationship between impurity phases of the materials and their photocatalytic activity was studied.

*Corresponding author. Fax: +82 54 279 5528.
E-mail address: jlee@postech.ac.kr (J.S. Lee).

0022-4596/$ - see front matter © 2007 Elsevier Inc. All rights reserved.
doi:10.1016/j.jssc.2007.01.008

2. Experimental

2.1. Materials preparation

$AgGaS_2$ was prepared by a conventional solid-state reaction. Stoichiometric amounts of Ag_2S (Aldrich, 99.9%) and Ga_2S_3 (10% excess, Aldrich, 99.99%) were mixed and ground in a *mortar* in the presence of ethanol and dried in an oven. Their pelletized form was annealed at different temperatures of 873–1073 K for 5 h under N_2 flow and the resulting materials were then ground in a *mortar* in the presence of ethanol. To remove defects and increase crystallinity, the powders (ca. 0.7 g) annealed at 1073 K were treated with H_2S at 873–1123 K for 3 h with a 40 vol% H_2S/He mixture flowing at 35 μmol/s.

2.2. Characterization with synchrotron radiation techniques

The crystalline phases of the materials were determined by synchrotron radiation powder X-ray diffraction (SR-XRD). The SR-XRD patterns were taken at 8C2 high-resolution powder diffraction beamline of Pohang Accelerator Laboratory (PAL) in Pohang, Republic of Korea. Scintillation counter detectors were rotated in a step of 0.01° around a flat sample-mounted stage, which was spinning to realize randomness of planes in materials during X-ray measurements. Full-profile structure refinements through Rietveld analysis were performed with *FULLPROF2 K* (Rodriguez-Carvajal, 1990).

The local structure around gallium in $AgGaS_2$ was characterized with XAFS. X-ray absorption measurements were conducted on beamline 7C1 of PAL (2.5 GeV; stored current of 120–180 mA). After treated at the desired temperatures, the materials were cooled to room temperature and their spectra were measured at room temperature in transmission mode. The radiation was monochromatized using a Si(111) double crystal monochromator and the incident beam was detuned by 15% using a piezoelectric translator in order to minimize contamination from higher harmonics, in particular, the third-order reflection of the silicon crystals. Since gallium metal foil was not available due to its low melting point, energy was calibrated with Ga_2O_3 and later, all spectra were re-calibrated with respect to *K*-edge energy of Ga by using FEFF calculations [15].

The obtained data were analyzed using the IFEFFIT suite of software programs [16] and the FEFF 8.2 code [15]. The detailed procedure for data analysis is described elsewhere [17,18,24]. The pre-edge background was removed by using a simple linear fit. The post-edge background function was approximated with a piecewise spline that could be adjusted so that the low-*R* components of pre-Fourier transformed data were minimized. After calculation of the extended X-ray absorption fine structure (EXAFS) function, k3-weighted $\chi(k)$ in momentum (k) space was Fourier transformed to obtain the radial structural function (RSF) in R space. A shell of interest in the RSF was back-transformed into the momentum space. The reference materials used as standards for fitting the experimentally derived RSFs were generated with the FEFF 8 code and the Fourier-filtered data were fitted in the momentum space.

2.3. Other characterizations

The optical properties of prepared materials were analyzed by UV–visible (VIS) diffuse reflectance (DR) spectrometer (Shimadzu, UV 2401). Morphologies of photocatalysts were investigated by field emission scanning electron microscopy (SEM, Hitachi, S-4200) and transmission electron microscope (JEOL JEM 2010F, field emission electron microscope) instrument operated at 200 kV.

2.4. Photocatalytic reactions

The photocatalytic reactions were carried out at room temperature under atmospheric pressure in a closed system using a Hg-arc lamp (500 W) equipped with a UV cut-off filter ($\lambda \geqslant 420$ nm). The rate of H_2 evolution was determined in an aqueous solution (100 ml) containing 0.1 g catalyst and 0.1 M Na_2S + 0.02 M Na_2SO_3. The evolved amounts of H_2 were analyzed by gas chromatography (TCD, molecular sieve 5-Å column and Ar carrier).

3. Results

3.1. Synthesis and characterization of p-type $AgGaS_2$ photocatalyst

Fig. 1 displays SR-XRD patterns of $AgGaS_2$ sample annealed at different temperatures of 873–1073 K under N_2 flow. Most reflections were indexed to the tetragonal phase $AgGaS_2$, of which cell constants are known as $a = 5.7572$ and $c = 10.3036$ Å in the literature [19]. However, as shown in Fig. 1, there exist some peaks due to impurity phases even for $AgGaS_2$ annealed at 1073 K.

The morphology of bulky $AgGaS_2$ particles prepared at various temperatures was observed by SEM images as shown in Fig. 2. The materials preserve irregular bulk particles with diameters of ca. 2–3 μm. As annealing temperature increases, the size becomes bigger and the surface becomes smoother. Thus, $AgGaS_2$ seems to obtain an improved crystallinity and bulkier geometry at high temperatures.

Fig. 3 shows the UV-diffuse reflection (UV-DR) spectra of $AgGaS_2$ annealed at 873–1073 K. The position of absorption edges was not much different. But, there exists absorption over the region of 500–700 nm due to vacancies or interstitial defects in the chalcopyrite lattice, which cause these materials to have poor crystal quality and poor optical property [20]. Fig. 4 shows the results of photocatalytic hydrogen production of aqueous electrolyte solution containing 0.1 M Na_2S and 0.02 M Na_2SO_3 as sacrificial reagents under visible light irradiation (using a

cutoff filter of $\lambda \geqslant 420$ nm for all catalysts). The rate of hydrogen evolution over $AgGaS_2$ prepared at the higher temperature (1073 K) was higher than those of photocatalysts prepared at lower temperatures (873–973 K). It is interesting to note that there was an apparent induction period of 1–2 h before the steady-state hydrogen evolution rate of $AgGaS_2$ was established for samples prepared at low temperatures (873–973 K). In contrast, the $AgGaS_2$ catalyst prepared at the high temperature (1073 K) did not show the induction period. The XRD pattern (not shown) of $AgGaS_2$ prepared at 973 K did not show any change before and after the photocatalytic reaction. Thus, there is no significant structure change during the induction period. It is possible that the surface defects are improved during this period by the reaction of the sample with S^{2-} ion in the solution.

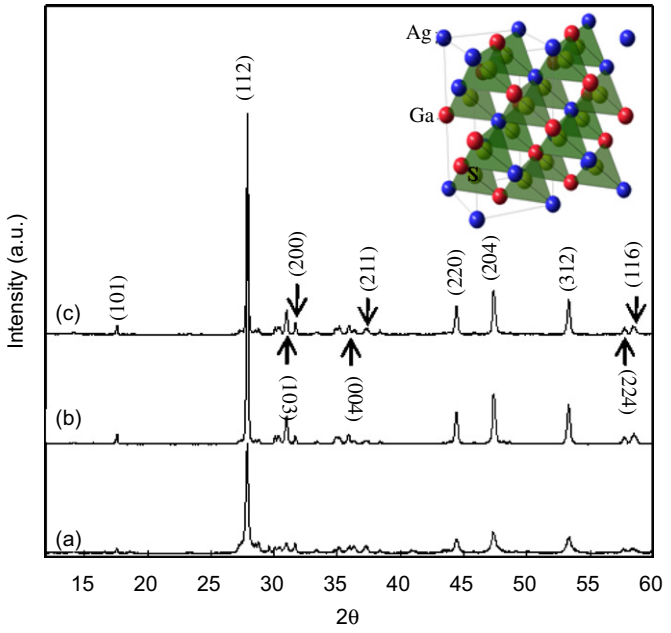

Fig. 1. Synchrotron radiation X-ray diffraction pattern of (a) $AgGaS_2$—873 K, (b) $AgGaS_2$—973 K, and (c) $AgGaS_2$—1073 K. All samples were heat-treated under N_2 flow for 5 h at the expressed temperature. The notated plane indices are those of tetragonal $AgGaS_2$ phase with the structure shown in the inset.

3.2. *Post-treatment of $AgGaS_2$ photocatalyst under H_2S gas flow*

In an attempt to remove vacancies or interstitial defects and to improve crystallinity, $AgGaS_2$ was treated at high temperatures of 873–1123 K under H_2S gas flow. Fig. 5 shows SR-XRD patterns before (A) and after (B) H_2S-treatment of the material, with a fit of full-profile structure refinements. Both β-Ga_2O_3 and $AgGaS_2$ phases were fitted in the Rietveld refinement mode, but Ag_9GaS_6 phase was fitted in the profile matching mode because only the space group and lattice parameters for Ag_9GaS_6 are known. Their calculated results are given in Table 1. The material before H_2S-treatment has a tetragonal structure of $AgGaS_2$ as the main structure and two impurity components of β-Ga_2O_3 and Ag_9GaS_6. When it was treated at 1123 K for 3 h under H_2S gas flow, the crystal was completely transformed into the main tetragonal structure without impurity components. The results of refinement in Table 1 shows that the lattice parameters for H_2S-treated $AgGaS_2$

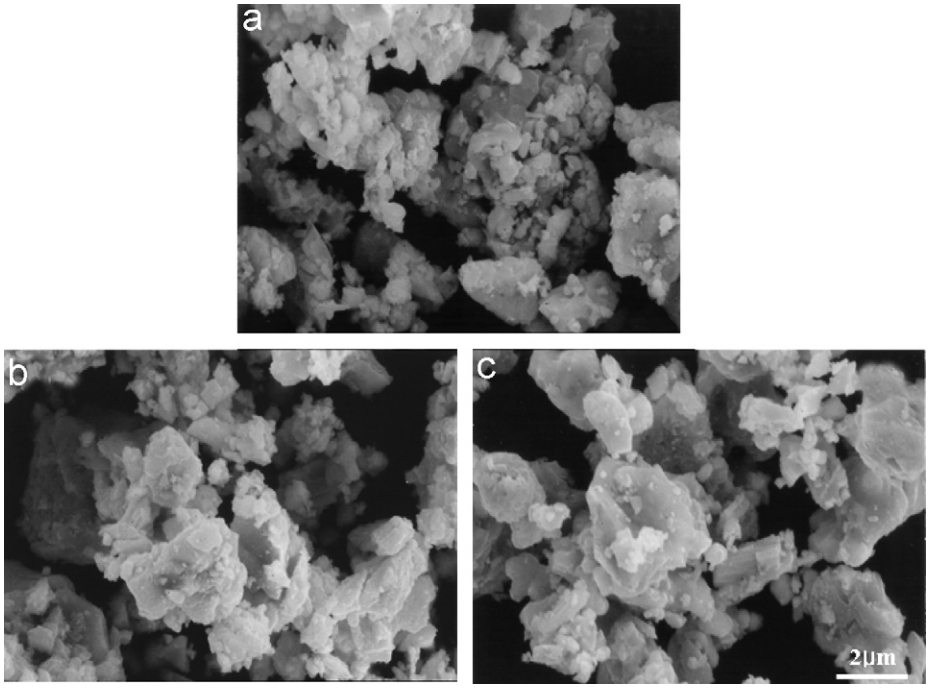

Fig. 2. SEM images of (a) $AgGaS_2$—873 K, (b) $AgGaS_2$—973 K, and (c) $AgGaS_2$—1073 K. All samples were heat-treated under N_2 flow for 5 h at the expressed temperature.

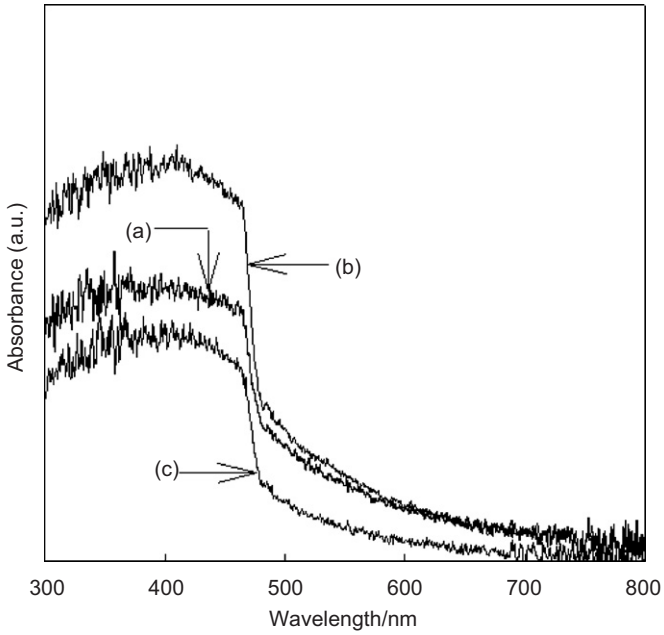

Fig. 3. UV–VIS diffuse reflectance spectra of (a) $AgGaS_2$—873 K, (b) $AgGaS_2$—973 K, and (c) $AgGaS_2$—1073 K. All samples were heat-treated under N_2 flow for 5 h at the expressed temperature.

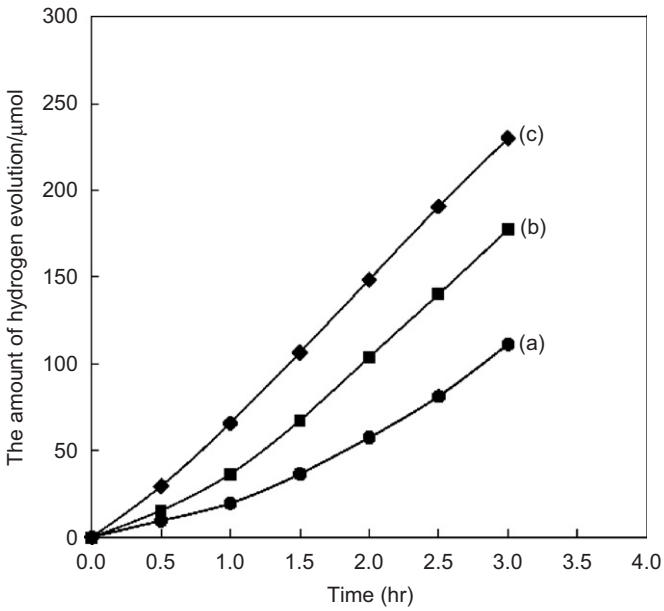

Fig. 4. Photocatalytic hydrogen production of (a) $AgGaS_2$—873 K, (b) $AgGaS_2$—973 K, and (c) $AgGaS_2$—1073 K. All samples were heat-treated under N_2 flow for 5 h at the expressed temperature. Catalysts: 0.1 g loaded 1 wt% Pt, electrolyte: 0.1 M Na_2S + 0.02 M Na_2SO_3.

material are in agreement with those of $AgGaS_2$ previously reported [19].

Fig. 6 shows the UV–Vis DR spectra for these samples. The positions of absorption edges were not much different for all samples. The untreated material (a) shows a diffuse absorption region (500–700 nm) due to vacancies or interstitial defects in the chalcopyrite lattice as discussed in the previous section. But, when this material was treated

Table 1
The results of structure refinement for before and after H_2S-tretated materials by Reitveld analysis

H_2S-treatment	Space group	Lattice parameters (a, b, c in Å, α, β, γ in deg)
Before		
$AgGaS_2$	$I\bar{4}2d$	5.76168, 5.76168, 10.2961, 90.0, 90.0, 90.0
Ag_9GaS_6	*Immm*	10.8321, 7.70382, 7.61941, 90.0, 90.0. 90.0
Ga_2O_3	$C12/m1$	2.23134, 3.03975, 5.80878, 90.0, 103.8, 90.0
After		
$AgGaS_2$	$I\bar{4}2d$	5.75978, 5.75978, 10.3018, 90.0, 90.0, 90.0

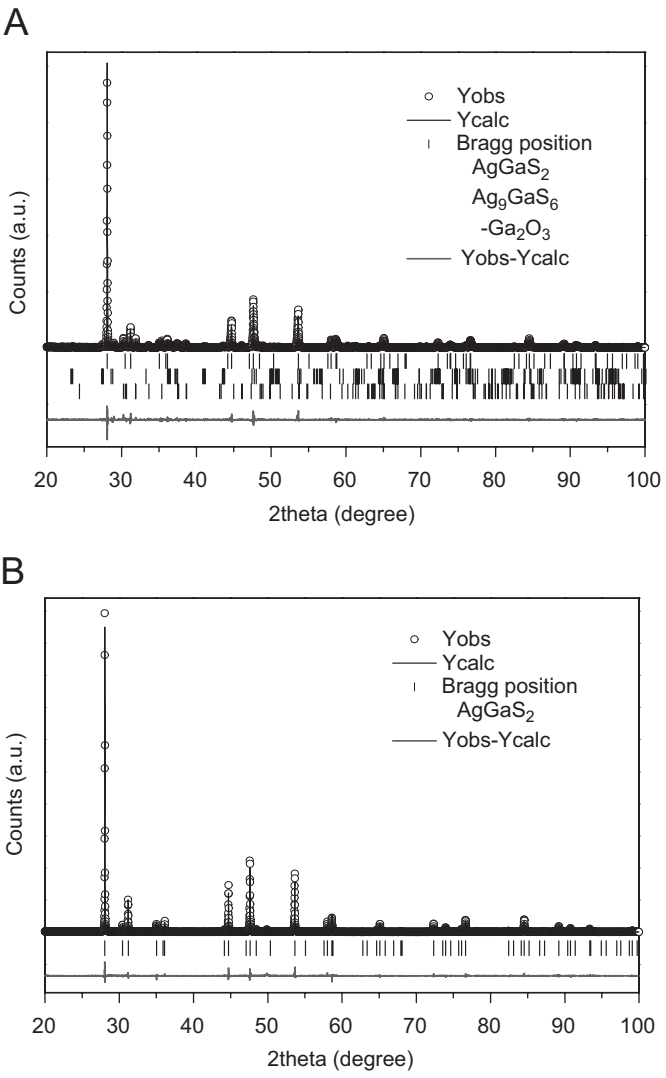

Fig. 5. Observed and calculated X-ray powder diffraction patterns of (A) untreated $AgGaS_2$ and (B) $AgGaS_2$ (H_2S—1123 K) are represented on the top by dots and a solid line, respectively. Vertical marks in the middle represent the calculated Bragg reflection angles. The trace on the bottom is a difference spectrum between the observed and calculated intensities.

at high temperatures under H_2S gas flow, absorption in the diffuse region (500–700 nm) decreased and sharper absorption spectra were observed. In particular, the H_2S

treatment increased absorption in blue to UV region of the spectrum. This result indicates that H_2S treatment drives $AgGaS_2$ into a purer and more crystalline form.

The morphologies of bulky $AgGaS_2$ particles treated at different temperatures under H_2S gas flow were observed by SEM as shown in Fig. 7. Their particle diameters are ca. 2–3 nm, almost the same as those of H_2S-untreated materials in Fig. 2. In untreated samples, $AgGaS_2$ particles were surrounded by the broken powders having sharp edges. But there were almost no broken particles and the surface became smoother for $AgGaS_2$ treated with H_2S gas at high temperatures.

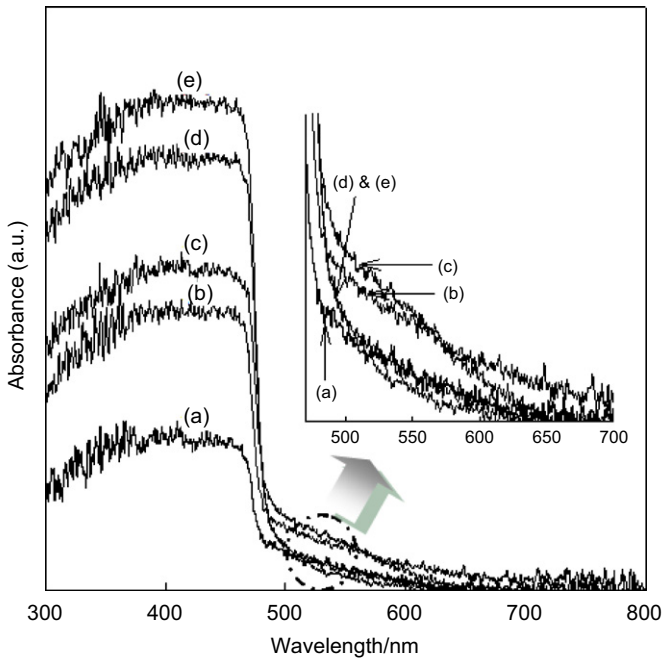

Fig. 6. UV–VIS diffuse reflectance spectra of (a) $AgGaS_2$—873 K, (b) $AgGaS_2$—973 K, (c) $AgGaS_2$—1073 K, and (d) $AgGaS_2$—1123 K. The samples of (a)–(d) were heat-treated under H_2S flow for 3 h at the indicated temperatures.

3.3. EXAFS of untreated and H_2S-treated $AgGaS_2$ photocatalysts

The radial structural functions (RSF) calculated from Ga *K*-edge EXAFS data are given in Fig. 8. Regardless of H_2S-treatment and treatment temperatures, all materials show a distinct peak at 1.2–2.3 Å, which could be assigned as the Ga–S interaction. However, the peaks above 2.3 Å change in a systematic manner with increasing H_2S-treatment temperatures. The peak at 2.3–3.3 Å decreases in magnitude of Fourier-transformed data as the sample is treated up to 1073 K under H_2S flow. At 1123 K, its RSF exhibits different features in the position of peaks as well as in intensity of peaks. The peak at 2.3–3.3 Å which was initially present in the untreated sample, almost disappears and a new peak at ca. 3.0–4.0 Å is observed. In consideration of the powder diffraction result in Fig. 5B, we fitted the experimental EXAFS data up to 4.07 Å with theoretically generated data of $AgGaS_2$. Fourier-filtered data and its best fit are shown in Fig. 9e and the quantitative results of EXAFS least-square fit are given in Table 2.

For other samples which were untreated and H_2S-treated up to 1073 K, only the first shell at 1.2–2.3 Å was inverse-Fourier transformed and fitted in *k*-space as shown in

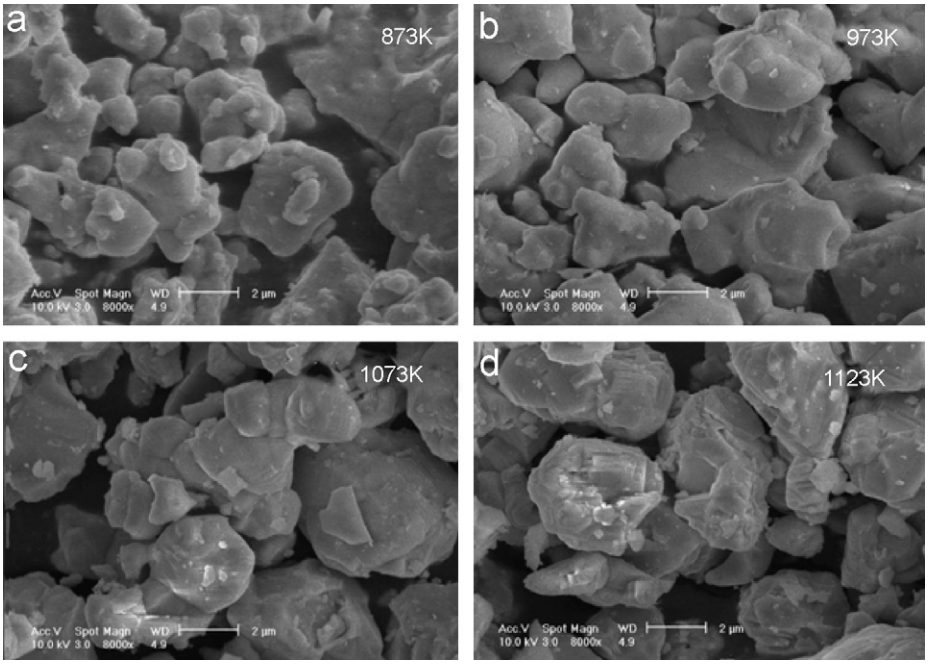

Fig. 7. SEM images of (a) $AgGaS_2$—873 K, (b) $AgGaS_2$—973 K, (c) $AgGaS_2$—1073 K, and (d) $AgGaS_2$—1123 K. The samples of (a)–(d) were heat-treated under H_2S flow for 3 h at the indicated temperature.

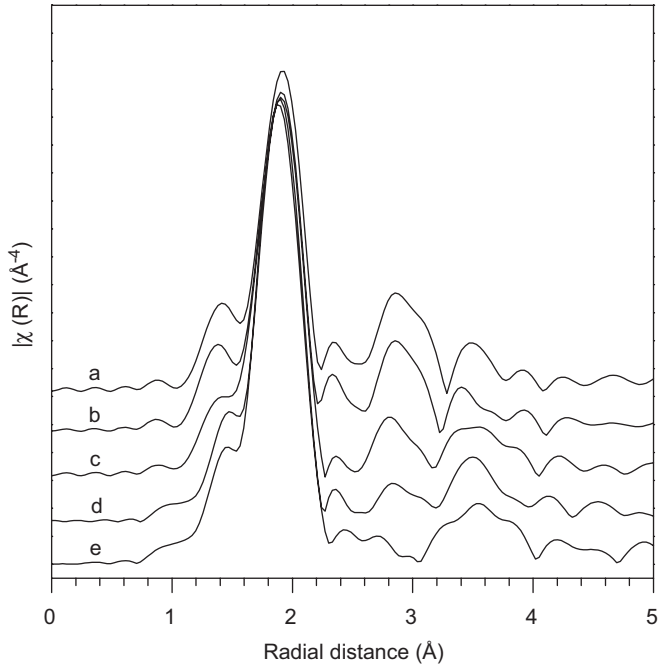

Fig. 8. k^3-weighted Fourier transformation about the Ga *K*-edges of (a) untreated $AgGaS_2$, (b) $AgGaS_2$—873 K, (c) $AgGaS_2$—973 K, (d) $AgGaS_2$—1073 K, and (e) $AgGaS_2$—1123 K. The samples of (b)–(e) were heat-treated under H_2S flow for 3 h at the indicated temperature.

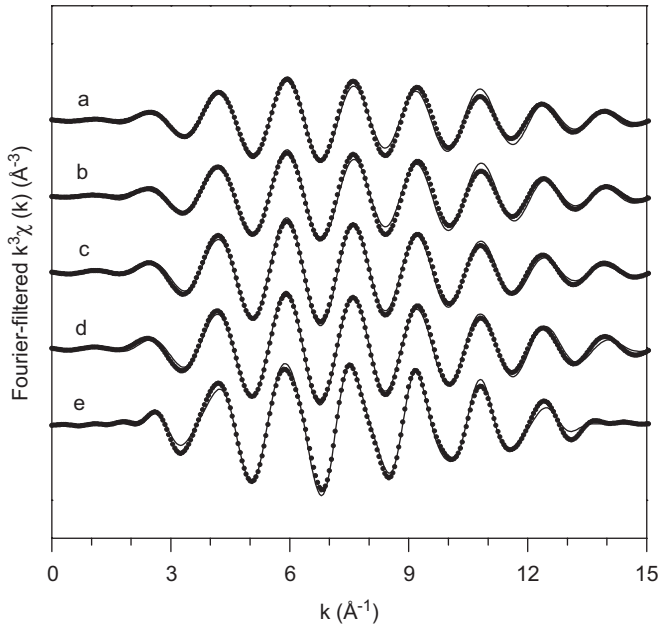

Fig. 9. Fourier-filtered EXAFS data (solid line) and their best-fits (dots) of (a) untreated $AgGaS_2$, (b) $AgGaS_2$—873 K, (c) $AgGaS_2$—973 K, (d) $AgGaS_2$—1073 K, and (e) $AgGaS_2$—1123 K. The samples of (b)–(e) were heat-treated under H_2S flow for 3 h at the indicated temperature.

Fig. 9a–d. The origin of the shell at 1.2–2.3 Å could be identified from comparison of the experimentally derived RSF with those of reference materials. Fig. 10 shows RSF of untreated material and those of β-Ga_2O_3 and $AgGaS_2$, of which the latter was theoretically synthesized by using the structure parameters obtained from the literature [19] with the FEFF 8.2 code [16]. Since the Debye–Waller factor was set to zero in the calculation for $AgGaS_2$, the intensity of peaks in RSF was relatively high and intense peaks appeared clearly up to 4.7 Å. The first shell of the untreated sample coincides with that of theoretical $AgGaS_2$ in both magnitude and the peak position. Therefore, we adopted the first Ga–S scattering of the theoretical $AgGaS_2$ RSF as the standard of fitting for untreated and H_2S-treated materials. The calculated structural parameters from the EXAFS fits are also given in Table 2. The Ga–S coordination number of untreated sample is 2.6 and that of H_2S-treated samples increases from 2.0 to 4.0 with increasing treatment temperatures.

As mentioned above, the features at higher shells in RSF (the peaks above 2.3 Å) show a systematic change during heat-treatment under H_2S flow. Thus, we need to clarify the detailed structures of β-Ga_2O_3 and $AgGaS_2$ with reference to Fig. 10. Since Ga^{3+} in β-Ga_2O_3 has two kinds of coordination, namely tetrahedral and octahedral, the distances between an absorber Ga and neighbor atoms are diverse as indicated in Table 3. In Table 3, the structural parameters of β-Ga_2O_3 were taken from the literature [21] and those of $AgGaS_2$ were calculated. β-Ga_2O_3 has two kinds of oxygen with average distances of 1.83 and 2.00 Å and those contributions are reflected on the first peak at 0.9–1.9 Å in RSF of Fig. 10. The distance of Ga–Ga varies from 3.04 to 3.45 Å, which corresponds to the peak at 2.3–3.3 Å in Fig. 10. On the other hand, the structure of $AgGaS_2$ is not complicated. The contribution from sulfur having a distance of 2.28 Å is reflected on the first peak and those from surrounding gallium, silver, and another sulfur at distances of 3.86, 4.07, and 4.45 Å, respectively, are expressed as the peaks at 3.3–4.7 Å in RSF of Fig. 10.

3.4. Photocatalytic performance of H_2S-treated $AgGaS_2$

Fig. 11 shows change in the evolution rate of H_2 from an aqueous solution containing 0.1 M Na_2S and 0.02 M Na_2SO_3 as sacrificial reagents under visible light irradiation (using a cutoff filter of $\lambda \geqslant 420$ nm for all catalysts) with respect to the temperature of H_2S treatment. The BET surface areas of the corresponding samples are also indicated. The rates of hydrogen evolution over H_2S treated $AgGaS_2$ at higher temperatures (1073 and 1123 K) were higher than those of photocatalysts untreated or treated at lower temperatures (873, 973 K). There is almost no correlation between BET surface areas and hydrogen evolution rates. Thus, it could be concluded that H_2S treatment is an effective method to obtain sulfide photocatalysts of high activity because it gives high purity and crystallinity of the photocatalyst.

Table 2
EXAFS least-square fitting results for untreated and H_2S-treated materials at different temperatures

H_2S treatment temp.	N_{Ga-S}	R_{Ga-S} (Å)	σ^2_{Ga-S} (Å^2)	ΔE_0 (eV)	R-factor
Untreated	2.6(4)[a]	2.29(1)	0.0043(10)	4.1	0.0173
873 K	2.8(4)	2.29(1)	0.0042(9)	2.7	0.0154
973 K	3.5(3)	2.29(1)	0.0051(6)	3.4	0.0071
1073 K	3.6(3)	2.29(1)	0.0047(6)	2.2	0.0047
1123 K[b]	4.0	2.29(1)	0.0044(1)	2.4	0.0141

[a]The value in parenthesis denotes the estimated error of the calculated parameter.
[b]Fitted to 4.07 Å with fixed coordination numbers which are already revealed with XRD of $AgGaS_2$. Its fit up to four shells results in $R_{Ga-Ag} = 3.88$ Å, $R_{Ga-Ga} = 3.88$ Å, and $R_{Ga-2Ag} = 4.09$ Å with $\sigma^2_{Ga-Ag} = \sigma^2_{Ga-2Ag} = 0.0213$ Å^2, $\sigma^2_{Ga-Ga} = 0.0114$ Å^2, $\Delta E_{0,Ga-Ag} = \Delta E_{0,Ga-2Ag} = -1.1$ eV, and $\Delta E_{0,Ga-Ga} = 3.1$ eV as well as parameters in the table.

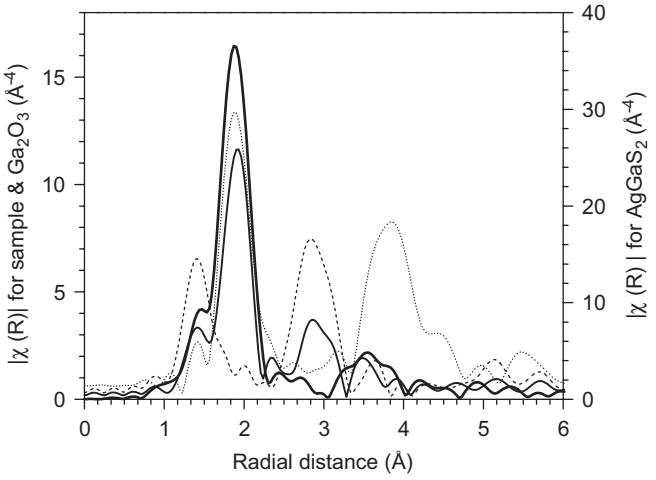

Fig. 10. Comparison of Fourier transformed data for untreated $AgGaS_2$ (solid line), H_2S-treated $AgGaS_2$ at 1123 K (thick solid line), Ga_2O_3 (dashed line), $AgGaS_2$ (dot line). $AgGaS_2$ (dot line) was theoretically synthesized by using of FEFF code.

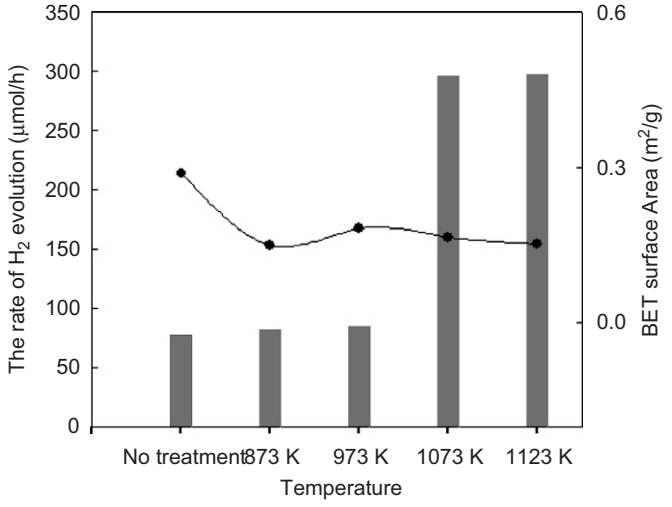

Fig. 11. The rate of photocatalytic hydrogen production of (a) untreated $AgGaS_2$, (b) $AgGaS_2$—873 K, (c) $AgGaS_2$—973 K, (d) $AgGaS_2$—1073 K, and (e) $AgGaS_2$—1123 K. The samples of (b)–(e) were heat-treated under H_2S flow for 3 h at the indicated temperature. Catalysts: 0.1 g loaded 1 wt% Pt, electrolyte: 0.1 M Na_2S + 0.02 M Na_2SO_3.

Table 3
Distances (Å) between a central atom Ga and neighbor atoms in the β-Ga_2O_3 and $AgGaS_6$ structures of Fig. 10

>-Ga_2O_3[a]		$AgGaS_6$	
Ga_I–$O_{,avg}$[b]	1.83	Ga–S	2.28
Ga_{II}–$O_{,avg}$[b]	2.00		
Ga_I–Ga_I(2)	3.04		
Ga_{II}–Ga_{II}(2)	3.04		
Ga_{II}–Ga_{II}(2)	3.11	Ga–Ag(4)	3.86
Ga_I–Ga_{II}	3.28	Ga–Ga(4)	3.86
Ga_I–Ga_{II}(2)	3.30	Ga–Ag(4)	4.07
Ga_I–Ga_{II}(2)	3.33	Ga–S(4)	4.45
Ga_I–Ga_{II}(2)	3.45		

[a]The data taken from Ref. [21]. The value in parenthesis is no. of atom pairs.
[b]Ga_I is tetrahedral and Ga_{II} is octahedral.

4. Discussion

A multicomponent sulfide photocatalyst $AgGaS_2$ prepared by a conventional solid-state reaction, showed an increased activity in hydrogen production from an aqueous electrolyte solution containing Na_2S and Na_2SO_3 under visible light as the annealing temperature in the preparation of materials increased. UV-DR spectra and powder diffraction patterns indicated the existence of impurity phases even for the material annealed at the highest employed temperature of 1073 K. From these results, it could be concluded that the preparation of $AgGaS_2$ photocatalyst must be optimized to obtain an improved photocatalytic activity. The post-synthetic H_2S treatment was an effective method to minimize the impurity phases for the sulfide photocatalyst and to bring superior photocatalytic performance. Thus, the $AgGaS_2$ samples treated at temperatures of 1073 and 1123 K under H_2S flow exhibited higher photocatalytic activity by factors of up to 4 compared with those of the untreated sample and H_2S-treated samples at lower temperatures of 873 and 973 K. In order to understand this significant promotional effect, the detailed investigation on change in the structure of materials during the H_2S-treatment was in order.

Synchrotron radiation techniques have proved to be powerful in revealing fine changes in the structure of condensed matters. The cell refinements for X-ray powder diffraction patterns demonstrated that untreated $AgGaS_2$ prepared at the annealing temperature of 1073 K consisted of three phases of $AgGaS_2$, Ag_9GaS_6, and Ga_2O_3. The evolution of β-Ga_2O_3 phase could be understood as the impurity originated from precursor Ga_2S_3, because both crystals are monoclinic with cell dimensions in order of $a > c > b$ [22,23]. The existence of Ag_9GaS_6 phase, for which the atomic positions in the structure have not been clearly revealed yet, could be controversial. But the phase diagram of silver–gallium–sulfur suggests that two additional phases of Ag_9GaS_6 and $Ag_2Ga_{20}S_2$ could co-exist together with chalcopyrite analog $AgGaS_2$ in the preparation of $AgGaS_2$ [23]. In fact, the lack of structural information on Ag_9GaS_6 made it impossible to determine the amount of three phases. On the other hand, the Rietveld analysis for H_2S-treated $AgGaS_2$ at 1123 K proved that the material had a chalcopyrite structure without impurity phases. Therefore, we could rationalize that the post-synthetic treatment under H_2S flow would change the structure of the solid.

The EXAFS, which provides direct information of local structure around a central atom, showed the changes in intensity and position of the second shell at 2.3–3.3 Å as well as in intensity of the first shell at 1.2–2.3 Å. In order to prevent EXAFS fit from over-calculating structural parameters, we considered only a Ga–S scattering for the fit of the first shell at 1.2–2.3 Å of all materials except for the one H_2S-treated at 1273 K. However, as mentioned above, the β-Ga_2O_3 phase was clearly identified in X-ray diffraction for untreated $AgGaS_2$. This result can also be partly supported by the RSF in Fig. 10, which shows that the position of the first peak in RSF coincides with that of Ga–S scattering of $AgGaS_2$, but its shoulder in a lower R implies a weak Ga–O interaction.

The systematic change in the second shell at 2.3–3.3 Å with increasing H_2S-treatment temperatures, gives us more insight regarding how impurity phases disappear. With examination of the imaginary portion of the Fourier transformed data, it would be possible to identify the back-scattering element contributing to a given peak. Fig. 12 displays both magnitude and imaginary functions for untreated $AgGaS_2$ (A) and β-Ga_2O_3 (B). The imaginary function of the second shell of untreated $AgGaS_2$ at 2.3–3.3 Å has the same feature as that of the second shell of β-Ga_2O_3 at 2.3–3.3 Å. It should be noted that the imaginary function is characteristic of the absorber–backscatterer pair, independent of the distance between the absorber and the backscatter or the coordination number of the backscatterer [24–26]. With the aid of FEFF simulation for β-Ga_2O_3 and Table 3, it can be concluded that the peaks at 2.3–3.3 Å in RSF reflects single scatterings of Ga–Ga and Ga–O and multiple scattering of Ga–O–O. Since the backscattering amplitude from a heavier element dominates contribution from a light backscatterer, we could state that the peak at 2.3–3.3 Å for untreated $AgGaS_2$ originates from the surrounding gallium in Ga_2O_3.

The intensity of the peak ca. at 2.3–3.3 Å for the untreated sample decreases and its position shifts to higher R, as the H_2S-treatment temperature increases. When the sample has a chalcopyrite structure without impurity phases (H_2S-treated sample at 1123 K), the peak appears at 3.6 Å with a significant intensity. Referring to Fig. 10 and Table 3, we can conclude that the peak is due to Ga–Ag, Ga–Ga, and Ga–Ag scatterings at distances of 3.86–4.07 Å. Therefore, as the H_2S-treatment temperature

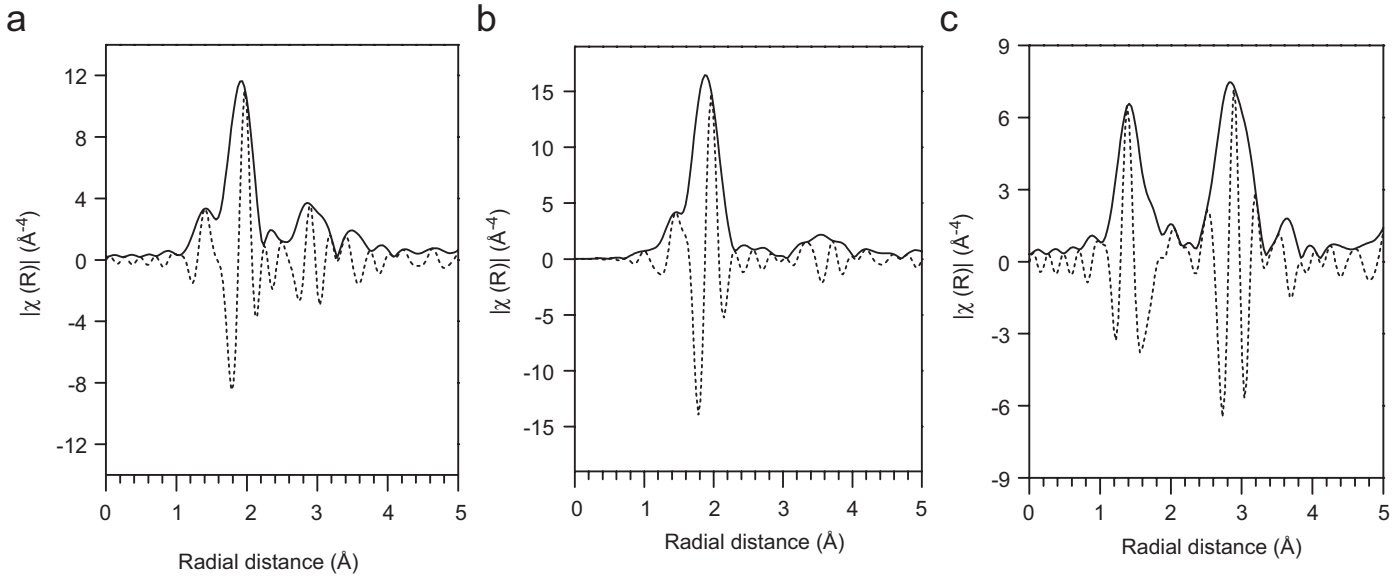

Fig. 12. k^3-weighted Fourier transformation about the Ga K-edges of (a) untreated $AgGaS_2$, (b) H_2S-treated $AgGaS_2$ at 1123 K, and (c) Ga_2O_3. The imaginary parts of Fourier transformed data are plotted as dashed lines.

increases, the contribution from the second shell of Ga_2O_3 is suppressed and that of $AgGaS_2$ becomes clearer because the content of the impurity phases is diminished. The EXAFS fitting results in Table 2 also indicate that the decrease of impurity phase causes the increased Ga–S coordination number with increasing of H_2S treatment temperature.

5. Conclusions

The $AgGaS_2$ photocatalysts prepared by heat-treatment at 873–1073 K under N_2 flow contained impurity phases identified as β-Ga_2O_3 and Ag_9GaS_6. Post-treatment of $AgGaS_2$ under H_2S flow at 1123 K resulted in the well-defined chalcopyrite structure without the impurity phases. The change in RSF of EXAFS and increase of Ga–S coordination number up to the stoichiometric coordination number of chalcopyrite structure revealed that as H_2S-treatment temperature increased, the impurity phases of Ga_2O_3 and Ag_9GaS_6 disappeared. Thus, obtained $AgGaS_2$ with no impurity and high crystallinity exhibited a high photocatalytic activity under visible light. This post-synthetic H_2S could also be applied for the synthesis of other sulfide-type photocatalysts with high activity.

Acknowledgments

This work was supported by the Hydrogen Energy R&D Center, one of the 21st Century Frontier R&D Program, funded by the Ministry of Science and Technology of Korea and the Brain Korea 21 Program endorsed by the Ministry of Education of Korea.

References

[1] N. Bubler, K. Meier, J.F. Reber, J. Phys. Chem. 88 (1984) 3261.
[2] S.A. Naman, M. Grätzel, J. Photochem. Photobiol. A 77 (1994) 249.
[3] J.S. Jang, W. Li, S.H. Oh, J.S. Lee, Chem. Phys. Lett. 425 (2006) 278.
[4] C.A. Linkous, N.Z. Muradov, S.N. Ramser, Int. J. Hydrogen Energy 20 (1995) 701.
[5] H. Kato, K. Asakura, A. Kudo, J. Am. Chem. Soc. 125 (2003) 3082.
[6] H.G. Kim, D.W. Hwang, J. Kim, Y.G. Kim, J.S. Lee, Chem. Commun. (1999) 1077.
[7] A.J. Frank, K. Honda, J. Phys. Chem. 86 (1982) 1933.
[8] I. Tsuji, H. Kato, A. Kudo, Angew. Chem. Int. Ed. 44 (2005) 3565.
[9] I. Tsuji, H. Kato, H. Kobayashi, A. Kudo, J. Am. Chem. Soc. 126 (2004) 13406.
[10] Z. Lei, W. You, M. Liu, G. Zhou, T. Takata, M. Hara, K. Domen, C. Li, Chem. Commun. 17 (2003) 2142.
[11] L. Brus, Appl. Phys. A 53 (1991) 465.
[12] J.L. Shay, B. Tell, H.M. Kasper, Appl. Phys. Lett. 19 (1971) 366.
[13] I. Choi, S. Eom, P.Y. Yu, J. Appl. Phys. 37 (2000) 3815.
[14] N. Yamamoto, K. Yokota, H. Horinaka, J. Cryst. Growth 99 (1990) 747.
[15] A.L. Ankudinov, C. Bouldin, J.J. Rehr, J. Sims, H. Hung, Phys. Rev. B 65 (2002) 104107.
[16] M. Newville, J. Synchrotron Radiat. 8 (2001) 322.
[17] S.H. Choi, J.S. Lee, J. Catal. 167 (1997) 364.
[18] E.D. Park, S.H. Choi, J.S. Lee, J. Phys. Chem. B 104 (2000) 5586.
[19] S.G. Abrahams, J.L. Bernstein, J. Chem. Phys. 59 (1973) 1625.
[20] N. Yamamoto, K. Yokota, H. Horinaka, J. Cryst. Growth 99 (1990) 747.
[21] S.J. Geller, Chem. Phys. 33 (1960) 676.
[22] J. Goodyear, G.A. Steigmann, Acta Crystallogr. 16 (1963) 946.
[23] G. Brandt, V. Kramer, Mater. Res. Bull. 11 (1976) 1381.
[24] D.E. Sayer, et al., in: D.C. Koningsberger, R. Prins (Eds.), X-ray absorption: Principles, Applications, Techniques of EXAFS, SEXAFS and XANES, Wiley, New York, 1988, p. 211.
[25] M. Vaarkamp, Catal. Today 39 (1998) 271.
[26] S.H. Choi, B. Wood, R. Benjamin, J.A. Ryder, A.T. Bell, J. Phys. Chem. B 107 (2003) 11843.